IET Journals
The Institution of Engineering and Technology

# Acoustic Diagnostics of Electrical Origin Fault Modes with Readily Available Consumer-Grade Sensors

ISSN 1751-8644
doi: 0000000000
www.ietdl.org

*Jarek Grebenik*[1*], *Chris Bingham*[2], *Saket Srivastava*[3]

[1,2,3] *School of Engineering, The University of Lincoln, Brayford Pool, Lincoln, LN6 7TS, United Kingdom*
** E-mail: jgrebenik@lincoln.ac.uk*

**Abstract:** Acoustic diagnostics, traditionally associated with mechanical fault modes, can potentially solve a wider range of monitoring applications. Typically, fault modes are induced purposefully by the researcher through physical component damage whilst the system is shutdown. This paper presents low-cost real-time fault diagnostics of a previously unreported acute electrical origin fault that manifests sporadically during system operation with no triggering intervention. A suitability study into acoustic measurements from readily available consumer-grade sensors for low-cost real-time diagnostics of audible faults, and a brief overview of the theory and configuration of the wavelet packet transform (including optimal wavelet selection methods) and empirical mode decomposition processing algorithms is also included. The example electrical origin fault studied here is an unpredictable current instability arising with the PWM-controller of a BrushLess DC motor. Experimental trials positively detect 99.9 % of the 1160 resultant high-bandwidth torque transients using acoustic measurements from a USB microphone and a smartphone. While the use of acoustic techniques for detecting emerging electrical origin faults remains largely unexplored, the techniques demonstrated here can be readily adopted for the prevention of catastrophic failure of drive and power electronic components.

## 1 Introduction

Acoustic condition monitoring is well reported for the assessment of operational integrity in many mechanically-based industrial applications with proven advantages over established techniques, e.g. vibration monitoring. Acoustic measurements can offer earlier and more accurate detection of emerging changes in system characteristics, improved cost-benefit trade-off, readily accessible transducers, ease of setup and operation, and no detrimental impact on nominal system integrity by virtue of employing remote sensors. Nevertheless, established confidence and reliance on traditional vibration-based techniques has largely impeded the uptake of acoustic-based counterparts for industrial system monitoring, despite their advantages [1]–[11]. Moreover, much of the published research employing acoustic methods focus on detecting mechanically-seeded, impact-based faults, usually identifying the initial acoustic front with specialist Acoustic Emission (AE) sensors [1]–[4], [11]–[14]. Roller Element Bearing (REB) faults are particularly prevalent due to their proportionally high failure rate and the breakdown of vibration-based methods at slow rotational speeds [15], [16].

Several authors [1]–[3], [11], [14], compare acoustic and vibration measurements experimentally and all largely agree on the relative advantages: the responsiveness to early-stage defects and greater diagnostic accuracy. A distinctive feature of AE detection is the traditional use of specialist transducers that require surface mounting to the component to detect ultrasonic frequencies which would otherwise rapidly attenuate through an air medium.

To-date consumer-grade sensors have been used largely for urban noise mapping and voice monitoring for medical and speech recognition purposes, although extensions to system monitoring have been previously reported by [17] where a mobile smartphone and tablet is used to detect air leakage from an industrial air compressor by differentiating healthy and leaking states through audio feature classification. A prior investigation in [18] diagnoses six common faults in REBs using very similar sensors to those given here. In laboratory conditions, the sensors achieved $100\,\%$ and $95\,\%$ accurate detection from the USB microphone and smartphone, respectively. The investigation demonstrated the suitability of such consumer-grade sensors for identifying mechanical faults. Nevertheless, the computational and memory technology present in mobile smartphones and tablets remains restrictive for complex real-time signal processing, currently preventing a black-box all-in-one solution.

Most reported fault detection techniques concerning induction motors focus on broken rotor bars, shorted windings or bearing defects, where the damage is often intentionally induced by the researcher as a laboratory exercise, whilst the system is offline. From a measurement perspective this provides data only in the extreme healthy and unhealthy states, whereas in real-world systems damage often emerges slowly as the components damage over a protracted period. Reviews of many such faults are given in [19]–[24] with notable comparisons of different methods. For instance, [25] diagnoses shorted stator coils using acoustic measurements analysed using a line spectrum frequency technique. A set of feature vectors are then calculated to be classified using a k-nearest neighbour algorithm that clusters similar vectors based on their Minkowski distance, allowing separation between healthy and fault condition classifications. More recently in [26], [27] differential diagnoses between several REB defects and a number of seeded physical structure changes that cause electrical faults, including shorted coils of auxiliary and main windings, shorted coils of auxiliary windings, broken rotor bars, and broken squirrel-cage ring on a single-phase induction motor using acoustics. Feature extraction is based on frequency vectors that help form a feature vector of between 1 and 22 frequency components. Training data allows a nearest neighbour classifier to then match new data to known values. The microphone used is inexpensive and readily available but the faults are identified offline and require relevant training data to provide correct diagnoses. [28] distinguish between broken rotor bars and several REB defects under various operating conditions by analysing a smoothed-pseudo Vigner-Ville distribution, and in [29] an interesting method to estimate three-phase induction motor torque from acoustic signals is presented. The authors utilise a six-level relational-dilation wavelet transform to preserve frequency resolution in the lower bands. During diagnostics of REB cage faults, broken rotor bars and single phasing faults, the authors show that the estimated torque from the acoustic signals is very close to the measured torque. A different approach to detect imbalance and bearing damage on an

induction motor is presented in [30] where triple-axis vibration measurements are analysed using a quaternion-based algorithm. This method is very computationally efficient using basic mathematical operations and not requiring space transformations which are commonplace when considering most other techniques. [31] detect a broken rotor bar with a Field-Programmable Gate Array (FPGA) implementation for faster, real-time processing of the motor current signal, while [32] diagnose stator inter-turn, dynamic eccentricity, and a combination of both using a finite element system model and frequency analysis from an oscilloscope. These latter investigations [31], [32], demonstrate the commercial requirement for fault detection in real-time, delivering near instant operator feedback, where all previously discussed literature reports post-trial analysis. Real-time detection allows timely intervention, possibly during the commissioning process, to ameliorate costly on-site operational faults and prevent catastrophic failure.

Despite the electrical basis of the above fault research, the failure mechanism continues to be a physical change from human intervention whilst the system is shutdown. In contrast, electrically-seeded faults, which are often transient and with unpredictable recurrence characteristics, are typically detected using three broad methods, viz. quantitative detection [33], high-frequency injection [34], [35], and Motor Current Signature Analysis (MCSA) [33], [36]. High-frequency injection operates on the same principle as sensorless motor control, where the saliency is used to estimate rotor position by superimposing a low-magnitude, high-frequency sinusoidal signal on the excitation voltage and measuring the high-frequency modulation changes. By profiling these to healthy and unhealthy states these signatures can be used to detect faults in the windings or elsewhere in the electromagnetic circuit [34], [36]. MCSA is a well-established technique that can be used to detect a wide-range of motor faults. However, it remains computationally intensive, requiring frequency analysis to determine harmonic components and fault signatures. This makes it unsuitable to detect transient characteristics [19], [20], [34], [36]. Nevertheless, this problem has been partially addressed in [23] where the authors detect bar breakage through transient MCSA realised through Continuous Wavelet Transform (CWT) and Discrete Wavelet Transform (DWT). Another example is given in [37] where stator currents are analysed using a four-level Wavelet Packet Transform (WPT) to detect broken rotor bar fault. However, the accuracy of fault detection deteriorates under light or no-load conditions. These electrically-based fault detection techniques, whilst effective and widely adopted, require specialist expertise, equipment, access to system components and can be difficult to install on established systems.

Building on previous research in [38], this paper demonstrates the suitability of acoustic measurements from consumer-grade sensors for the real-time detection of sporadic, unpredictable and transient current instabilities of electrical origin. Specifically, as an example case study, a permanent magnet BLDC motor drive system that exhibits sporadic current instabilities which only occur during well-bounded operating regimes (at relatively high rotor speeds under light load conditions) is considered in this instance. It is notable that a $25\,\%$ change in the proportional gain element of the current controller negates the unstable operation thereby indicating that the instability is controller induced, and a result of the non-linear interaction of the motor electrical parameters, parasitic components and digital controller realisation. By way of example, Fig. 1 shows each phase current supplied to the BLDC motor under no-load operation (hence the voltage overhead is insufficient to produce classical 'flat-topped' current waveforms). In this case, four discrete periods of unstable controller induced current oscillations that remain for the commutation period can be seen. These unstable events have the potential to propagate to drive system failure, poor performance or possible demagnetisation of the motor (if the commutation sequence is disrupted). Although a single significant event could initiate these failure modes, a more likely scenario is that multiple minor events would occur over a prolonged period, causing long-term damage that would otherwise remain undetected. The current instabilities induce an audible, mechanical torque transient within the motor, producing an acoustic signature in the audible range ($20\,\mathrm{Hz}$ to $20\,\mathrm{kHz}$) commensurate with typical PWM frequencies and AC sources, and making consumer-grade acoustic transducers appropriate. This differs from prior investigations that typically employ vibration sensors or specialised piezoelectric transducers, surface mounted for higher-frequency pickup (typically $100\,\mathrm{kHz}$ to $1\,\mathrm{MHz}$). Such sensor systems are of comparatively high-cost, require complex specialist setup and operation (low-noise transmission and amplification, and fast data acquisition), are more susceptible to operational damage, and are intrusive to the system under test. Electrical origin fault modes are traditionally diagnosed electrically with techniques such as MCSA. Furthermore, to date, research has focussed on detecting faults caused by mechanical changes to the system. The method presented here is widely applicable to both mechanical and electrically-seeded faults that result in an audible signature. The particular case considered in this paper represents one practical example. The key contributions of this paper are:

- the diagnosis of electrical origin faults where the failure mode is unseeded (i.e. not by human intervention) and manifests sporadically during continuous system operation,
- the proposed use of consumer-grade acoustic sensors that are readily available for low-cost continuous real-time monitoring,
- a brief comparison of methods for optimal selection of the mother wavelet when using wavelet transformations.

## 2 Underlying Principles

### *2.1 Acoustic Transducers*

Consumer-grade acoustic transducers are designed to measure longitudinal pressure waves in air within the audible frequency range (consistent with the music and telephonic industries). These integrated sensor systems are highly-developed and mass produced, and are therefore widely available, low-cost and easy to use. Four main acoustic sensor categories exist; capacitive, inductive, piezoelectric and optical. Most surface mounted 'research-grade' sensors are piezoelectric, whereas consumer-grade sensors usually operate on capacitive principles as follows. Typically, a thin gold-coated mylar diaphragm forms a flexible capacitor plate that moves with respect to the other plate in response to acoustic pressure waves, Fig. 2. This changes the capacitance, usually in the region of 10

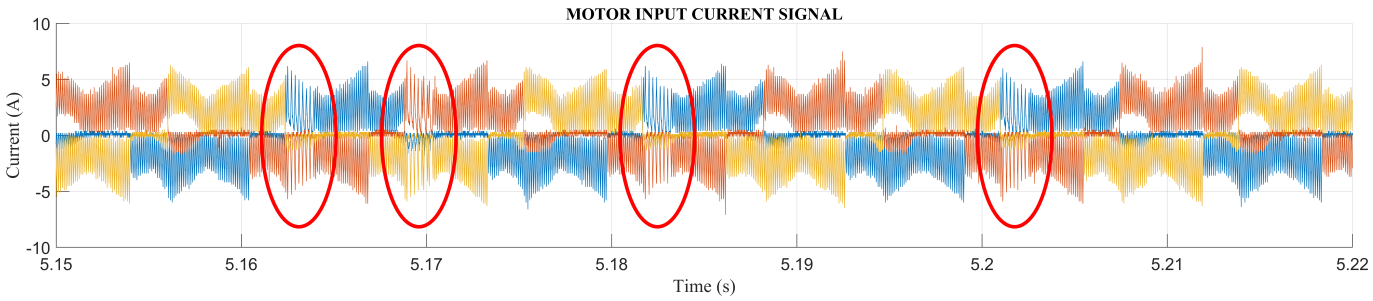


**Fig. 1**: Three-phase BLDC motor currents with four distinct current instabilities circled.

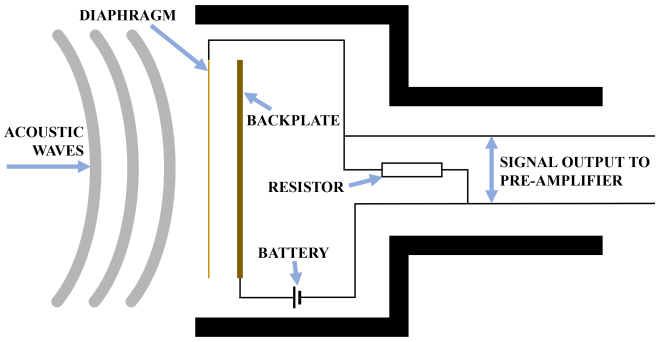


**Fig. 2**: Diagram of a simple capacitive microphone circuit.

to 50 pF. A phantom power source provides a DC voltage (usually 48 V) that pulls the diaphragm taut. As the capacitance changes, the small voltage fluctuations across a high load resistor are amplified and measured as the audio signal. These remote sensors commonly exhibit directional sensitivity that are depicted as polar patterns of four primary types: omni-direction, bi-directional, cardioid or super-cardioid. The cardioid pattern is most suitable in this case and for condition monitoring since it is most sensitive at the front with reduced lateral and minimal rear pick-up [39].

Unlike surface-mounted counterparts these consumer-grade sensors suffer from signal attenuation through the air which is more pronounced at higher frequencies. They are also prone to superimposed noise from a variety of external sources, and careful selection of the feature extraction algorithm is therefore necessary.

### 2.2 *Fault Signature Extraction*

Separating the acoustic fault signature from unwanted noise can prove challenging in a real-world environment. Noise from the surrounding environment and auxiliary electrical sources, combined with signal attenuation through medium transmission, sensor imperfections, and analogue to digital conversion, can result in the fault signatures becoming buried. The goal of feature extraction is to isolate as much fault information as possible with minimal computation overhead.

Mathematically, there are three primary domains in which signals are traditionally analysed. Firstly is the time domain with a plethora of mathematical techniques and algorithms available, ranging in complexity from basic mathematical operations such as multiplication through to composite sequential operations forming algorithmic analysis. Secondly, the Fourier transform or variations thereof, which converts a time or spatial domain signal to a frequency representation. In signal processing the Fast Fourier Transform (FFT) is commonly utilised to determine underlying frequency content. The third domain, known as the time-frequency domain, allows the study of both time and frequency information simultaneously. However, there is a trade-off in resolution between time and frequency domains. Fig. 3 illustrates the concept of how these different domains can trade-off resolution. Although excellent resolution can be achieved in both time and frequency using techniques such as Short-Time Fourier Transform (STFT), a significantly disproportionate amount of computation is required, making this technique unsuitable for low-cost real-time continuous processing and for larger datasets. An advantage of so-called wavelet transforms is in the configuration of the domain resolutions, making the algorithm significantly more efficient whilst still achieving the required resolution performance.

Fault detection algorithms can be broadly categorised into those that can detect continuous (e.g. a mechanically worn component or a pressurised leak) or transient (e.g. a mechanical impact such as damage to the race of a roller bearing) faults. Identifying a continuous fault is relatively straightforward as marked differences between healthy and unhealthy states would usually be evident in the frequency spectrum. Equally in the time domain a change from a healthy to an unhealthy state may also be evident. However, transient

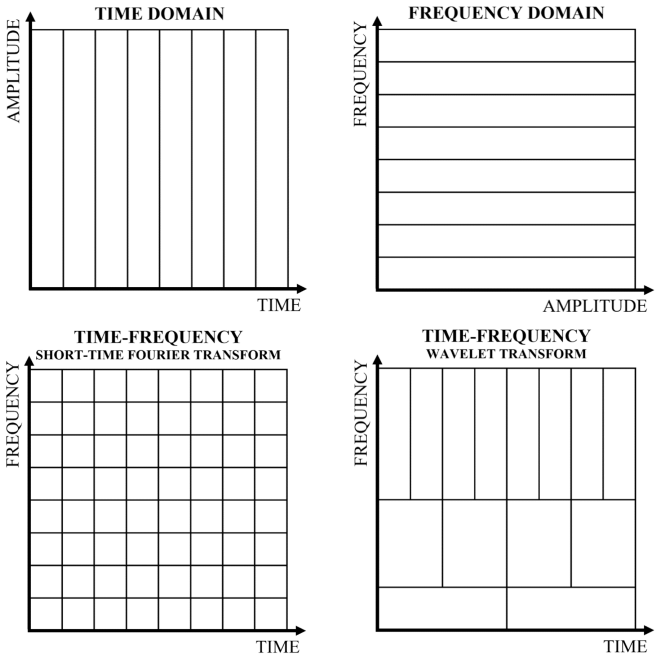


**Fig. 3**: Diagram illustrating the resolution differences between time, frequency, and time-frequency domains.

fault types can prove more challenging as the fault signature is often hidden in the time domain and may only result in very low-level changes in the frequency domain. A time-frequency algorithm can then be used to better identify such conditions. When considering different feature extraction methods, it is critical that the nature of the fault features are well-understood. In this case, as is common with transient fault detection, the signature is of high frequency and short time duration. Therefore, an optimal detection algorithm would seek to reveal frequency changes with respect to time, as corroborated in [3], [5]–[10], [12], [40]–[45].

There are many well-known time-frequency techniques such as the STFT, spectrogram analysis, wavelet transform, Wigner distribution, Wigner-Ville, Choi-Williams, and Hilbert-Huang Transform (HHT), from which many variations are derived. For this work, two feature extraction algorithms, WPT and Empirical Mode Decomposition (EMD), are chosen for comparative purposes. These techniques are prominent in the field and their suitability and excellent performance for such applications are well-documented. Aiming to demonstrate the suitability of real-time acoustic signal processing for previously unexplored fault types (of electrical origin and with no physical change to nominal system integrity), it is desirable to use WPT and EMD as they are commonly used and well-understood in the wider industry to provide an initial investigation into this novel application sector [44]. An overview of both techniques is now provided along with some insight on why these specific variations are particularly suited to this application.

*2.2.1 Wavelet Theory:* The wavelet transform can be considered a dynamic extension to the classical Fourier transform which uses the sum of complex exponentials, but instead employs a dyadic dilation of a scaling function and translation of a mother wavelet function (example given in Fig. 4). The CWT of a finite energy signal $x(t)$ is the result of convolving that signal with a dyadic scaling and translation of a mother wavelet $\Psi(t)$ of the form:

$$W_{(\alpha,b)} = \alpha^{\frac{1}{2}} \int_{-\infty}^{\infty} x(t)\Psi * \left(\frac{t-b}{\alpha}\right) dt \qquad (1)$$

where $W_{(\alpha,b)}$ is the wavelet coefficient, $\alpha$ is the dyadic scaling, $b$ is the dyadic translation and $\Psi$ is the mother wavelet.

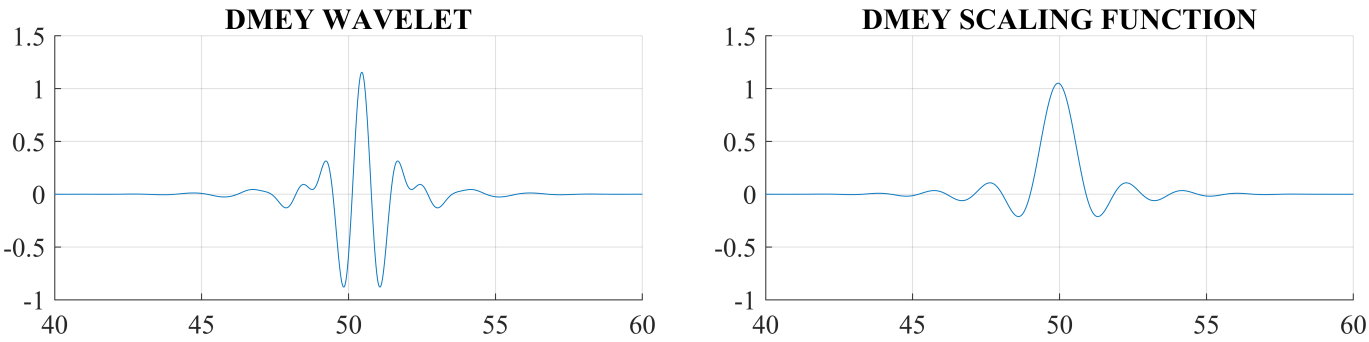


**Fig. 4**: The dmey mother wavelet and scaling function. Axes units not relevant here.

A true CWT requires an infinite number of functions that generate an infinite number of coefficients, which is impossible to realise practically. Letting $\alpha = 2^m$ and $b = n2^m$ (where $m$ and $n$ are integers), the CWT becomes discrete and forms an orthonormal basis set;

$$\Psi_{(m,n)}(t) = 2^{-\frac{m}{2}}\Psi(2^{-m}t - n) \tag{2}$$

allowing realisable calculation overhead. The base scale is usually a fractional power of 2 in the form $2^{j/v}$, where $j$ represents the number of scales and $v$ represents the fidelity of each scale (sometimes known as the number of 'voices per octave'). The resulting number of coefficients remains very high - an $M$ by $N$ matrix, where $N$ is the input signal length and $M$ is the number of scales.

The DWT discretises the scale to $2^{j/1}$ with only a single 'voice per octave' and base scale of 2. This results in the number of coefficients being equal to an $L + 1$ by $N$ matrix, where $L$ is the decomposition level. The DWT convolves the original signal with a low pass filter $h(n)$ and high pass filter, $g(n)$, and downsamples by a factor of 2. $h(n)$ and $g(n)$ are a coarse discretisation of the dyadic scaling and wavelet function, and take the form:

$$h(n) = \frac{1}{\sqrt{2}}\langle\varphi(t), \varphi(2t - n)\rangle \tag{3}$$

$$g(n) = \frac{1}{\sqrt{2}}\langle\Psi(t), \Psi(2t - n)\rangle = (-1^n)h(1 - n) \tag{4}$$

where $\varphi(t)$ is the dyadic scaling function.

This results in approximate coefficients $cA_1$ and detail coefficients $cD_1$. The process can be repeated on the approximation coefficients to give a multi-level decomposition, as depicted in Fig. 5. Reconstruction of the signal involves upsampling by two and convolving the approximation and detail coefficients with low and high pass reconstruction filters respectively, giving the real approximation and detail that are then summed [7], [44].

The WPT follows the same principle but additionally decomposes the 'detail path' and the 'approximation path' at each level. This

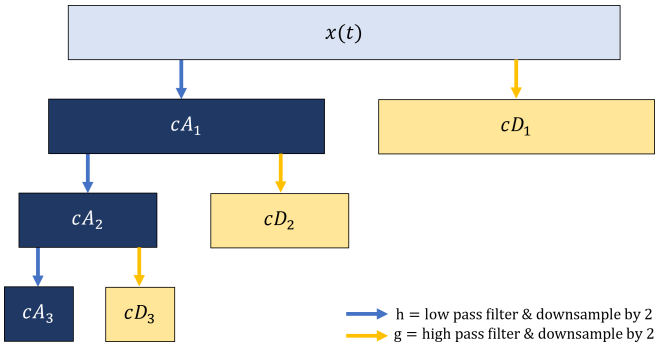


**Fig. 5**: Example three level DWT. Original time domain signal is $x\,(t)$, and signal reconstruction uses $cA_3$ and $cD_1$ to $cD_3$.

results in an even wavelet packet tree shown in Fig. 6. Frequency folding which occurs with WPT results in low pass filtered signals containing information on the high frequency content. Consequently, the reconstruction order is aligned to the frequency order by inverting the position of each right-hand branch (illustrated by the red swap arrows and text). For example, at the third level the natural order is 0, 1, 2, 3, 4, 5, 6, 7 but the frequency order becomes 0, 1, 3, 2, 7, 6, 4, 5 [7], [44].

Although the CWT offers high-fidelity, it is excessive for this purpose and the computational resources required are generally too large for low-cost real-time continuous processing. The DWT or WPT offers a sparse representation of the signal providing compression, but also reconstruction of the original signal from the approximation and detail coefficients. The additional terminal nodes of WPT over DWT allows deeper analysis of the different frequencies and the complex reconstruction can use specific terminal nodes facilitating unparalleled isolation of fault information, revealing the abrupt changes in hidden frequencies [3], [6], [7], [44].

*2.2.2 Empirical Mode Decomposition Theory:* EMD forms the first part of the Hilbert-Huang Transform [46] and is a time domain signal decomposition method particularly suited to analysing non-linear and non-stationary systems and signals. Each decomposition level begins with a sifting operation where smooth upper and lower envelopes of the signal based on local maxima and minima (using cubic spline interpolation) are generated. The mean of the two envelopes $m_1$ is then subtracted from the original signal to give the first sifted component, $h_1 = x(t) - m_1$. The second sifting iteration treats $h_1$ as the input and $m_{11}$ is the mean of the new input upper and lower envelopes giving $h_{11} = h_1 - m_{11}$. This process is repeated $k$ times, $h_{1k} = h_{1(k-1)} - m_{1k}$ until a termination criterion is reached. This forms the first Intrinsic Mode Function (IMF), $c_1 = h_{1k}$ which is subtracted from the original signal to give the first residue $r_1 = x(t) - c_1$. The residue is then treated as the input and the sifting process repeats $j$ times until the stoppage criterion, $r_j = r_{(j-1)} - c_j$ is reached. Various stoppage criteria can be used, such as a standard deviation match, a predefined threshold, energy difference tracking or S-number (the number of consecutive sifting iterations where the number of zero crossings and extrema are the same or differ by one). The IMFs are oscillatory functions with higher IMF decomposition levels revealing subsequently lower frequencies. All the IMFs are the same length as the original signal and they must satisfy the two criteria below such that their superposition will reconstruct the original signal:

- the number of IMF extrema (the sum of the maxima and minima) and the number of zero crossings must either be equal or differ at most by one;
- at any point of an IMF the mean value of the envelope defined by the local maxima and the envelope defined by the local minima shall be zero.

It is well known that EMD is prone to mode mixing and aliasing issues with more intermittent signals, resulting in IMFs that are devoid of physical meaning. EMD also degrades when multiple concurrent data points form a flat or non-oscillatory part of the signal

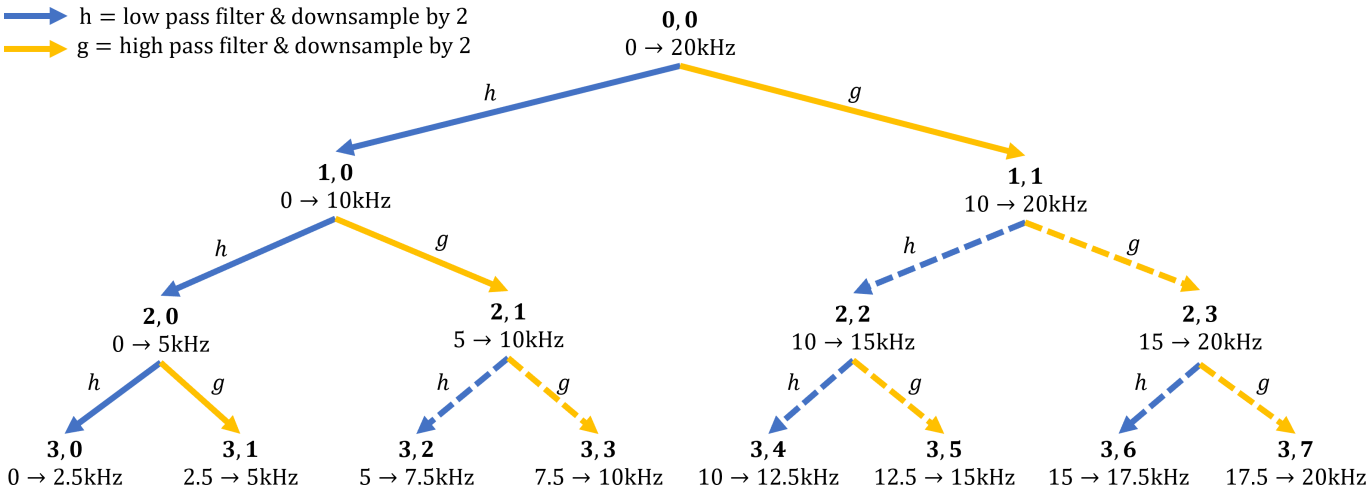


**Fig. 6**: Example three level WPT tree showing the frequency range corresponding to each node coordinate. Dashed lines show the additional branches of WPT compared to DWT.

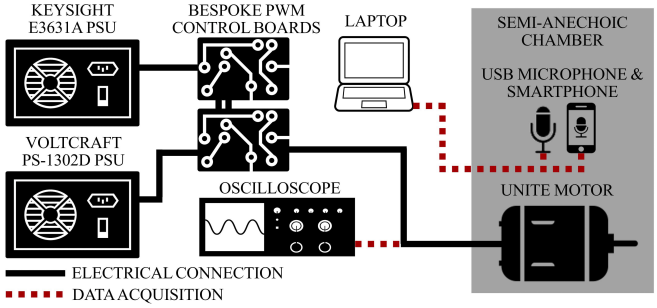


**Fig. 7**: Experimental setup diagram.

e.g. a square wave. To counter these disadvantages Ensemble Empirical Mode Decomposition (EEMD) [47] adds white noise to the input signal and then takes the ensemble mean of multiple outputs to form a single IMF. Accuracy is increased by using more ensembles, cancelling the white noise. However, this is computationally intensive and makes EEMD unsuitable for low-cost real-time processing. Further, since acoustic signals are highly-oscillatory EEMD would not provide any significant advantage over conventional EMD. Although EMD remains a time domain algorithm, it does provide an analysis of pseudo-time-frequency information. However, the result is devoid of physical meaning and the IMFs are not precisely orthogonal. For the acoustic signals analysed here, EMD can imprecisely reveal the short-time transient frequency changes with excellent detection accuracy providing isolation of an empirically-derived fault signature.

## 3 Experimental Setup

A three-phase BLDC 36 V 1600 W Unite MY1020 motor is powered through a bespoke digital current controller. Internal Hall-effect sensors are used to facilitate commutation. Consumer-grade acoustic transducers, specifically an Audio-Technica AT2020 USB+ microphone and a Samsung Galaxy S7 smartphone using WO Mic, are both positioned $\approx$10 cm from the motor with their sensitive planes directed toward the motor. A setup diagram is given in Fig. 7. Both acoustic sensors have their own inbuilt analogue to digital converter and connect digitally for continuous real-time sampling at 48 kHz with 16-*bit* resolution using Matlab. In parallel with the sampling, Matlab discretises the data into packets and processes each one using the feature extraction techniques, delivering real-time analysis every 0.2 s. A posteriori knowledge of the instability duration (approximately 1.5 ms) is used to define the system refresh rate of 5 Hz; sufficiently long to capture entire instability periods but fast enough to prevent damage to the motor drive. The three motor phase currents are measured using three isolated high-bandwidth Hall-effect current sensors, sampled at 250 kHz with 16-*bit* resolution on an oscilloscope. The high sampling rate allows inter-PWM current characteristics to be captured. The motor and acoustic sensors are sited in a semi-anechoic chamber, ensuring minimal background noise. Nevertheless, signal processing is still required to adequately separate the fault information from unwanted motor noise.

### *3.1 Wavelet Packet Transform Configuration*

Optimal selection of the mother wavelet is critical to the performance of the WPT and is dictated by the similarity of the wavelet shape to the signal of signature through dilation and translation. In other words, through dilation and translation how well can the wavelet match the signal or signature. There is no defined method to determine this, and researchers have devised various quantitative measures, all fundamentally based on experimentation and a posteriori knowledge of relevant signatures. Typically, a selection of different wavelets are tested for various quantitative performance factors such as maximum energy, minimum entropy, minimum reconstruction error, cross-correlation to name a few. In [48], five attributes (energy, Shannon-entropy, signal power to noise power ratio, mean square error, and maximum absolute squared deviation) are evaluated for twenty-six different wavelets. Three separate weighting schemes are applied to the attributes using the analytic hierarchy process (based on pairwise comparison matrix of the attributes). Each weighting scheme revealed a performance ranking order of the wavelets analysed where the highest-ranking wavelet is deemed to deliver the best performance for the given application. A slightly simpler approach is given in [49], where the maximum energy to Shannon-entropy ratio is used as a measure of wavelet performance. This method is undertaken for the investigation in this paper, as the acoustic fault signature is known to be of a transient nature within the normal operational characteristics of the motor. Although for certain applications it may be necessary to undertake a further comparative study of information measures (joint entropy, conditional entropy, mutual informal, relative entropy and comparative information entropy for example), it is unnecessary in this case due to the transient nature of the fault signature. Therefore, the best maximum energy to Shannon-entropy ratio is used to select the wavelet. Sixty different wavelet types from the Haar, Daubechies, Symlets, Coiflets, Biorthogonal, Reverse-Biorthogonal, Discrete approximation of Meyer (dmey) and Fejer-Korovkin families are analysed; revealing the dmey wavelet (from Fig. 4) to be most suitable for these signals.

The required number of decomposition levels is visually determined through inspection of the terminal node coefficients using the Matlab wavelet analyser; aiming to maximise the isolation of the fault signature from unwanted noise. This analysis, Fig. 8 shows

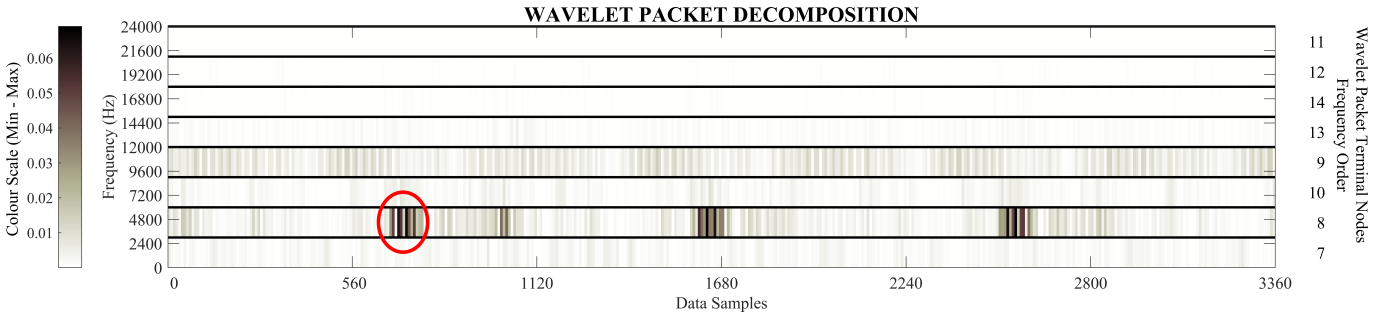


**Fig. 8**: Microphone data dmey 3-level WPT terminal node coefficients. The instability information from Fig. 1 can be seen as dark patches in terminal node [3,1] or 8. First one circled for clarity.

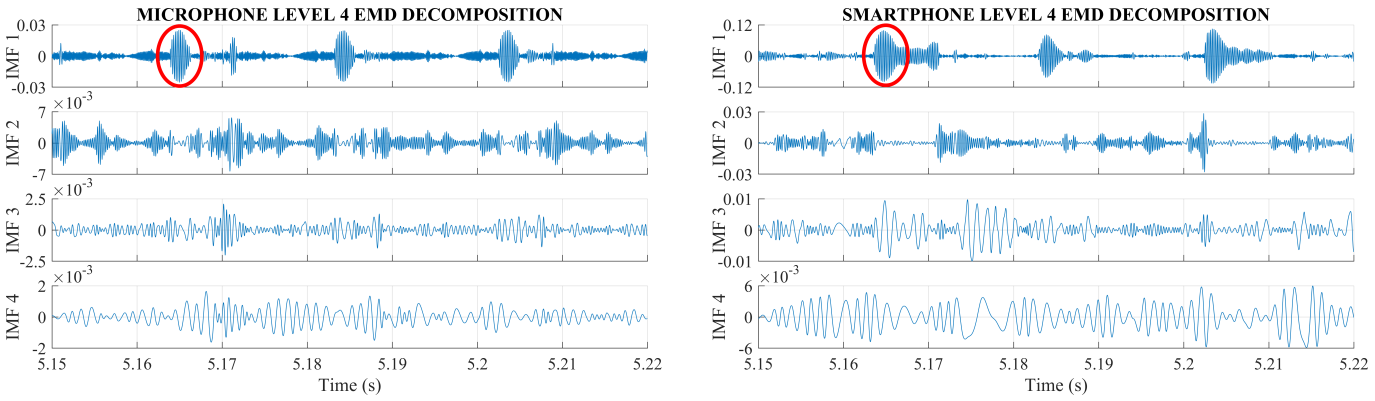


**Fig. 9**: EMD 4-levels with microphone data on the left, and smartphone data on the right. Only relative amplitude are significant on the IMFs (in descending order), with the red circle marking the first of four instabilities.

excellent fault signature isolation into terminal node $[3, 1]$ or $8$. The higher coefficient values are colour mapped darker. The original signal is reconstructed from these coefficients thus excluding most of the unwanted noise and erroneous frequencies and delivering the fault information signature. Reconstruction is realised through upsampling by two and convolving the approximation and detail coefficients with low and high pass reconstruction filters respectively which gives the real approximation and detail that is summed together.

### *3.2 Empirical Mode Decomposition Configuration*

An empirical approach is used to establish the required number of decomposition levels. Both microphone and smartphone measurements are initially decomposed into four levels giving the four IMFs shown in Fig. 9. As the fault information is expected to be high-frequency it would likely be contained in the early IMFs. The default stopping criterion is based on standard deviation matching and a maximum of 2000 sifting iterations allow normal operation of the sifting process.

The results, Fig. 9, shows the majority of the fault information is preserved in IMF 1. Hence, only a 2-level decomposition is necessary; providing the first IMF for further analysis and a residue signal containing everything else i.e. the remaining noise. Interestingly, there is no apparent information relating to the instabilities in any of the remaining IMFs indicating only higher-frequency fault information.

### *3.3 Fault Diagnostic Method*

In summary, the acoustic measurements from the USB microphone and smartphone sensors are pre-processed using the WPT and EMD algorithms described above delivering four sensor / algorithm combinations, Fig. 10. A standard peak finding approach is the final step to detect the instabilities in each pre-processed signal. Detection is qualified using an amplitude threshold based on the standard deviation of each processed signal (data from a preliminary test run). Windowing discretises individual instabilities using a lower limit separation of $0.02\,\mathrm{s}$ (sufficiently long to distinguish between instability periods, but short enough to not class two separate instabilities together as a single entity). Fig. 10 shows the detection threshold line along with the identified instability start and end points.

## 4 Experimental Results

The results from three experimental trials are now presented with analysis of the sensor and feature extraction algorithm relative performance, and detection rates of the electrically-seeded instabilities.

### *4.1 Consumer Transducer Performance*

Firstly, the number of unstable periods for each trial are counted from the motor phase current measurements, and are compared in Table 1 against the four sensor and algorithm combinations (top row of each trial). The bottom row of each trial is a percentage of the sensor/algorithm detection rate against the actual occurrences. The green values show that the microphone/WPT combination provided $100\,\%$ accuracy in detecting the fault periods during trials 1 and 2, with only a single missed instability period during trial 3. This excellent performance is further highlighted in Table 2, where the mean percentage of correct detection across all three trials reveals the performance of the sensors, algorithms and combinations. The USB microphone marginally outperforms the smartphone by $1.7\,\%$, achieving an overall detection rate of $99.9\,\%$. This is attributable to its larger, open diaphragm, compared to the smartphone which has a water-resistant microphone within a small aperture. Nevertheless, the smartphone performance remains impressive considering the relative disadvantages. The semi-anechoic environment minimises

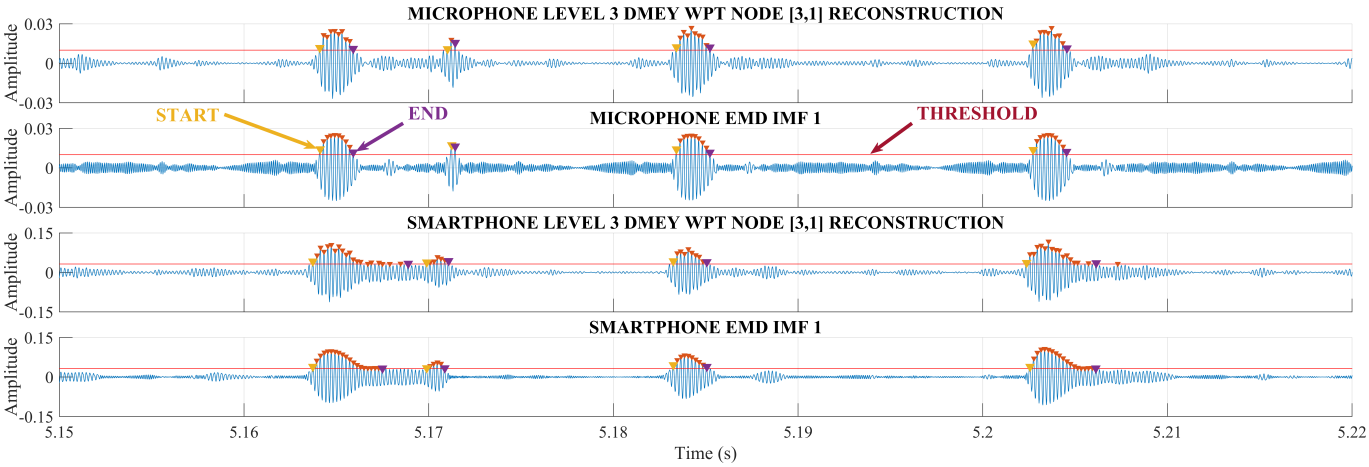


**Fig. 10**: Processed signals showing almost exclusively fault information. The peak detection threshold is shown by the horizontal red line with detected peaks marked in red, and the start and end of each discrete instability in yellow and purple respectively.

**Table 1** The total number of unstable features found for each trial using the phase current measurements as a reference for the acoustically detected faults. Blue indicates that some unstable periods were missed, orange indicates false positive detections (which also result in percentages over 100 %), and green shows the best performance.

| TRIAL | INSTABILITY PERIODS DURING TRIAL | ACOUSTIC DETECTOR PERFORMANCE | | | |
|---|---|---|---|---|---|
| | | MICROPHONE | | SMARTPHONE | |
| | | WPT | EMD | WPT | EMD |
| 1 | 327 | 327 | 326 | 309 | 290 |
| | | 100.0% | 99.7% | 94.5% | 88.7% |
| 2 | 690 | 690 | 658 | 685 | 668 |
| | | 100.0% | 95.4% | 99.3% | 96.8% |
| 3 | 143 | 142 | 142 | 147 | 145 |
| | | 99.3% | 99.3% | 102.8% | 101.4% |
| TOTAL | 1160 | 1159 | 1126 | 1141 | 1103 |
| | | 99.9% | 97.1% | 98.4% | 95.1% |

background noise and is partially responsible for the high detection rates achieved. Even so, the results do demonstrate the potential benefits of the proposed methodology.

### *4.2 Fault Signature Extraction Algorithm Performance*

Results in Tables 1 and 2 show that the WPT algorithm outperforms EMD in detection performance by isolating the fault signature entirely into one terminal node. In some cases, EMD failed to separate events that occurred in close proximity, resulting in multiple instabilities being classed as one by the detection algorithm.

Regarding real-time processing, the mean data packet processing times provide an indication of computational efficiency for the feature extraction algorithms as given in Table 3. The times are normalised to the system refresh rate (0.2 s) for clarity. Processing times are seen to be very close to the system refresh rate. A slower processing rate is not suitable for real-time systems as the time lag will continue to increase and the system will run out of memory. Both feature extraction algorithms performed well overall, with EMD exhibiting the slowest and fastest processing. However, WPT proved to be consistently faster, delivering the fastest mean processing time.

**Table 2** Correct detection percentage across all three trials.

| | WPT | EMD | MEAN |
|---|---|---|---|
| MICROPHONE | 99.9% | 97.1% | 98.5% |
| SMARTPHONE | 98.4% | 95.1% | 96.1% |
| MEAN | 99.1% | 96.1% | |

**Table 3** Mean processing times across all trials normalised to the system refresh rate.

| TRIAL | WPT | EMD |
|---|---|---|
| 1 | -0.31 | 1.69 |
| 2 | -0.55 | -2.37 |
| 3 | -0.52 | -0.18 |
| MEAN | -0.46 | -0.28 |

## 5 Conclusion

This paper presents the use of acoustic measurements for low-cost real-time detection of an acute electrical origin fault mode that manifests sporadically under well-bound operating conditions on a BrushLess Direct Current (BLDC) motor drive system. The example fault mechanism investigated is a transient current instability that arises in the motor supply from the controller due to the non-linear interaction of the PWM-controller parameters, parasitic components and digital controller realisation. This case study

verifies that acoustic measurements are capable of detecting electrical origin faults. Low-cost continuous real-time acoustic monitoring is realised through the readily available consumer-grade sensors employed, specifically a USB microphone and portable smartphone. These sensor types can be easily and readily adopted to solve a wide variety of real-world condition monitoring and fault detection requirements in both mechanical and electrical systems and of both mechanical and electrical origin fault modes. Across the three experimental trials undertaken, 1160 discrete unstable controller induced current oscillations were present. An investigation into the suitability of consumer-grade sensors and feature extraction algorithm performance, (specifically combinations of a USB microphone and smartphone acoustic transducers with Wavelet Packet Transform (WPT) or Empirical Mode Decomposition (EMD) feature extraction) revealed that all combinations delivered excellent performance. However, it was the USB microphone and WPT feature extraction that performed best - correctly identifying 1159 (99.9 %) of the instabilities. This is attributed to the larger diaphragm of the USB microphone and optimal selection of the analysing wavelet by the highest energy to Shannon-entropy ratio method. Although the USB microphone performed marginally better, the smartphone offers the potential to become an all-in-one future diagnostic tool given the obvious advantages of being established, easily accessible, relative low-cost, self-powering, remote from the system, and with internet and other communication built in. This research may provide the stimulus for the widespread adoption of consumer-grade sensors and smartphone technology for fault detection and monitoring of both mechanical and electrical systems and fault modes.

## References


[1] T. H. Loutas, G. Sotiriades, I. Kalaitzoglou, *et al.*, "Condition monitoring of a single-stage gearbox with artificially induced gear cracks utilizing on-line vibration and acoustic emission measurements," *Applied Acoustics*, vol. 70, pp. 1148–1159, 9 2009. [Online]. Available: https://doi.org/10.1016/j.apacoust.2009.04.007.

[2] B. Eftekharnejad, M. R. Carrasco, B. Charnley, *et al.*, "The application of spectral kurtosis on acoustic emission and vibrations from a defective bearing," *Mechanical Systems and Signal Processing*, vol. 25, pp. 266–284, 1 2011. [Online]. Available: https://doi.org/10.1016/j.ymssp.2010.06.010.

[3] F. Hemmati, W. Orfali, and M. S. Gadala, "Roller bearing acoustic signature extraction by wavelet packet transform, applications in fault detection and size estimation," *Applied Acoustics*, vol. 104, pp. 101–118, 2016. [Online]. Available: https://doi.org/10.1016/j.apacoust.2015.11.003.

[4] H. Li, F. Xu, H. Liu, *et al.*, "Incipient fault information determination for rolling element bearing based on synchronous averaging reassigned wavelet scalogram," *Measurement*, vol. 65, pp. 1–10, 2015. [Online]. Available: https://doi.org/10.1016/j.measurement.2014.12.032.

[5] M. Amarnath and I. R. P. Krishna, "Empirical mode decomposition of acoustic signals for diagnosis of faults in gears and rolling element bearings," *IET Science, Measurement and Technology*, vol. 6, pp. 279–287, 4 2011. [Online]. Available: https://doi.org/10.1049/iet-smt.2011.0082.

[6] P. Konar and P. Chattopadhyay, "Bearing fault detection of induction motor using wavelet and support vector machines (SVMs)," *Applied Soft Computing*, vol. 11, pp. 4203–4211, 6 2011. [Online]. Available: https://doi.org/10.1016/j.asoc.2011.03.014.

[7] N. G. Nikolaou and I. A. Antoniadis, "Rolling element bearing fault diagnosis using wavelet packets," *NDT&E International*, vol. 35, pp. 197–205, 3 2002. [Online]. Available: https://doi.org/10.1016/S0963-8695(01)00044-5.

[8] K. Feng, Z. Jiang, W. He, *et al.*, "Rolling element bearing fault detection based on optimal antisymmetric real laplace wavelet," *Measurement*, vol. 44, pp. 1582–1591, 9 2011. [Online]. Available: https://doi.org/10.1016/j.measurement.2011.06.011.

[9] W. He, Z.-N. Jiang, and K. Feng, "Bearing fault detection based on optimal wavelet filter and sparse code shrinkage," *Measurement*, vol. 42, pp. 1092–1102, 7 2009. [Online]. Available: https://doi.org/10.1016/j.measurement.2009.04.001.

[10] P. K. Kankar, S. C. Sharma, and S. P. Harsha, "Rolling element bearing fault diagnosis using wavelet transform," *Neurocomputing*, vol. 74, pp. 1638–1645, 10 2011. [Online]. Available: https://doi.org/10.1016/j.neucom.2011.01.021.

[11] K. R. Al-Balushi, A. Addali, B. Charnley, *et al.*, "Energy index technique for detection of acoustic emissions associated with incipient bearing failures," *Applied Acoustics*, vol. 71, pp. 812–821, 9 2010. [Online]. Available: https://doi.org/10.1016/j.apacoust.2010.04.006.

[12] D. Mba and R. B. K. N. Rao, "Development of acoustic emission technology for condition monitoring and diagnosis of rotating machines; bearings, pumps, gearboxes, engines and rotating structures," *The Shock and Vibration Digest*, vol. 38, pp. 3–16, 1 2006. [Online]. Available: https://doi.org/10.1177/0583102405059054.

[13] T. J. Holroyd, "The application of AE in condition monitoring," in *Proceedings of the British Institute of Non-Destructive Testing Conference on Condition Monitoring (BINDT CM2005)*, British Institute of Non-Destructive Testing (BINDT), vol. 47, Cambridge, United Kingdom: Holroyd Instruments Ltd., 2005, pp. 481–485.

[14] A. M. Al-Ghamd and D. Mba, "A comparative experimental study on the use of acoustic emission and vibration analysis for bearing defect identification and estimation of defect size," *Mechanical Systems and Signal Processing*, vol. 20, pp. 1537–1571, 7 2006. [Online]. Available: https://doi.org/10.1016/j.ymssp.2004.10.013.

[15] Z. Mo, J. Wang, H. Zhang, *et al.*, "Vibration and acoustics emission based methods in low-speed bearing condition monitoring," in *Proceedings of the Prognostics and System Health Management Conference*, IEEE, Chongqing, China: IEEE, 2018, pp. 871–875.

[16] B. Van Hecke, J. Yoon, and D. He, "Low speed bearing fault diagnosis using acoustic emission sensors," *Applied Acoustics*, vol. 105, pp. 35–44, 2016. [Online]. Available: https://doi.org/10.1016/j.apacoust.2015.10.028.

[17] N. K. Verma, J. V. Singh, M. Gupta, *et al.*, "Windows mobile and tablet app for acoustic signature based machine health monitoring," in *Proceedings of the 9th International Conference on Industrial and Information Systems (ICIIS)*, IEEE, Gwalior, India: IEEE, 2014, pp. 1–6.

[18] J. Grebenik, Y. Zhang, C. Bingham, *et al.*, "Roller element bearing acoustic fault detection using smartphone and consumer microphones - comparing with vibration techniques," in *Proceedings of the 17th International Conference on Mechatronics - Mechatronika (ME)*, IEEE, Prague, Czech Republic: IEEE, 2016, pp. 1–7.

[19] A. Siddique, G. S. Yadava, and B. Singh, "A review of stator fault monitoring techniques of induction motors," *IEEE Transactions On Energy Conversion*, vol. 20, pp. 106–114, 1 2005. [Online]. Available: https://doi.org/10.1109/TEC.2004.837304.

[20] S. Nandi, H. A. Toliyat, and X. Li, "Condition monitoring and fault diagnosis of electrical motors - a review," *IEEE Transactions On Energy Conversion*, vol. 20, pp. 719–729, 4 2005. [Online]. Available: https://doi.org/10.1109/TEC.2005.847955.

[21] Y. Liu and A. M. Bazzi, "A review and comparison of fault detection and diagnosis methods for squirrel-cage induction motors - state of the art," *ISA Transactions*, vol. 70, pp. 400–409, 2017. [Online]. Available: https://doi.org/10.1016/j.isatra.2017.06.001.

[22] O. E. Hassan, M. Amer, A. K. Abdelsalam, *et al.*, "Induction motor broken rotor bar fault detection techniques based on fault signature analysis – a review," *IET Electric Power Applications*, vol. 12, pp. 895–907, 7 2018. [Online]. Available: https://doi.org/10.1049/iet-epa.2018.0054.

[23] J. Pons-Llinares, V. Climente-Alarcón, R. Puche-Panadero, *et al.*, "Bar breakage detection on squirrel cage induction motors via transient motor current signal analysis based on the wavelet transform, a review," Departamento de Ingeniería Eléctrica, Universidad Politécnica de Valencia, España, 2017.

[24] Y. Tian, D. Guo, K. Zhang, *et al.*, "A review of fault diagnosis for traction induction motor," in *Proceedings of the 37th Chinese Control Conference (CCC)*, Wuhan, China, 2018, pp. 5763–5768.

[25] A. Glowacz, "Diagnostics of synchronous motor based on analysis of acoustic signals with the use of line spectral frequencies and k-nearest neighbor classifier," *Archives of Acoustics*, vol. 39, no. 2, pp. 189–194, 2014. [Online]. Available: https://doi.org/10.2478/aoa-2014-0022.

[26] A. Glowacz, W. Glowacz, Z. Glowacz, *et al.*, "Early fault diagnosis of bearing and stator faults of the single-phase induction motor using acoustic signals," *Measurement*, vol. 113, pp. 1–9, 2018. [Online]. Available: https://doi.org/10.1016/j.measurement.2017.08.036.

[27] A. Glowacz, "Fault diagnosis of single-phase induction motor based on acoustic signals," *Mechanical Systems and Signal Processing*, vol. 117, pp. 65–80, 2019. [Online]. Available: https://doi.org/10.1016/j.ymssp.2018.07.044.

[28] W. Li and C. K. Mechefske, "Detection of induction motor faults - a comparison of stator current, vibration and acoustic methods," *Journal of Vibration and Control*, vol. 12, pp. 165–188, 2 2006. [Online]. Available: https://doi.org/10.1177/1077546306062097.

[29] B. P. Sangeetha and S. Hemamalini, "Rational-dilation wavelet transform based torque estimation from acoustic signals for fault diagnosis in a three phase induction motor," *IEEE Transactions on Industrial Informatics (Early Access)*, 2018. [Online]. Available: https://doi.org/10.1109/TII.2018.2874463.

[30] J. L. Contreras-Hernandez, D. L. Almanza-Ojeda, S. Ledesma-Orozco, *et al.*, "Quaternion signal analysis algorithm for induction motor fault detection," *IEEE Transaction on Industrial Electronics (Early Access)*, 2019. [Online]. Available: https://doi.org/10.1109/TIE.2019.2891468.

[31] A. Ordaz-Moreno, R. d. J. Romero-Troncoso, J. A. Vite-Frias, *et al.*, "Automatic online diagnosis algorithm for broken-bar detection on induction motors based on discrete wavelet transform for FPGA implementation," *IEEE Transactions On Industrial Electronics*, vol. 55, pp. 2193–2202, 5 2008. [Online]. Available: https://doi.org/10.1109/TIE.2008.918613.

[32] J.-K. Park and J. Hur, "Detection of inter-turn and dynamic eccentricity faults using stator current frequency pattern in IPM-type BLDC motors," *IEEE Transactions On Industrial Electronics*, vol. 63, pp. 1771–1780, 3 2016. [Online]. Available: https://doi.org/10.1109/TIE.2015.2499162.

[33] M. Riera-Guasp, J. A. Antonino-Daviu, and G.-A. Capolino, "Advances in electrical machine, power electronic, and drive condition monitoring and fault detection: state of the art," *IEEE Transactions On Industrial Electronics*, vol. 62, pp. 1746–1759, 3 2015. [Online]. Available: https://doi.org/10.1109/TIE.2014.2375853.

[34] F. Immovilli, C. Bianchini, E. Lorenzani, *et al.*, "Evaluation of combined reference frame transformation for interturn fault detection in permanent-magnet multiphase machines," *IEEE Transactions On Industrial Electronics*, vol. 62, pp. 1912–1920, 3 2015. [Online]. Available: https://doi.org/10.1109/TIE.2014.2348945.

[35] J. Arellano-Padilla, M. Sumner, and C. Gerada, "Winding condition monitoring scheme for a permanent magnet machine using high-frequency injection," *IET Electric Power Applications*, vol. 5, pp. 89–99, 1 2011. [Online]. Available: https://doi.org/10.1049/iet-epa.2009.0264.

[36] B. Sen and J. Wang, "Stator interturn fault detection in permanent-magnet machines using PWM ripple current measurement," *IEEE Transactions On Industrial Electronics*, vol. 63, pp. 3148–3157, 5 2016. [Online]. Available: https://doi.org/10.1109/TIE.2016.2515560.

[37] Y. Cekic and L. Eren, "Broken rotor bar detection via four-band wavelet packet decomposition of motor current," *Electrical Engineering*, vol. 100, pp. 1957–1962, 3 2018. [Online]. Available: https://doi.org/10.1007/s00202-017-0674-4.

[38] J. Grebenik, C. Bingham, and S. Srivastava, "Continuous acoustic monitoring of electrical machines; processing signals from USB microphone & mobile smartphone sensors detecting dc motor controller fault," in *Proceedings of the 5th International Conference on Control, Decision & Information Technologies (CoDIT)*, IEEE, Thessaloniki, Greece: IEEE, 2018, pp. 677–682.

[39] K. Farrar, "Soundfield microphone - design and development of microphone and control unit," *Wireless World*, pp. 48–50, 1979.

[40] M. A. F. Pimentel, D. A. Clifton, L. Clifton, *et al.*, "A review of novelty detection," *Signal Processing*, vol. 99, pp. 215–249, 2014. [Online]. Available: https://doi.org/10.1016/j.sigpro.2013.12.026.

[41] A. Rai and S. H. Upadhyay, "A review on signal processing techniques utilized in the fault diagnosis of rolling element bearings," *Tribology International*, vol. 96, pp. 289–306, 2016. [Online]. Available: https://doi.org/10.1016/j.triboint.2015.12.037.

[42] G. F. Bin, J. J. Gao, X. J. Li, *et al.*, "Early fault diagnosis of rotating machinery based on wavelet packets - empirical mode decomposition feature extraction and neural network," *Mechanical Systems and Signal Processing*, vol. 27, pp. 696–711, 2012. [Online]. Available: https://doi.org/10.1016/j.ymssp.2011.08.002.

[43] Y. Lei, J. Lin, Z. He, *et al.*, "A review on empirical mode decomposition in fault diagnosis of rotating machinery," *Mechanical Systems and Signal Processing*, vol. 35, pp. 108–126, 1 - 2 2013. [Online]. Available: https://doi.org/10.1016/j.ymssp.2012.09.015.

[44] M. M. M. H. Da Costa Cesar; Kashiwagi, "Rotor failure detection of induction motors by wavelet transform and fourier transform in non-stationary condition," *Case Studies in Mechanical Systems and Signal Processing*, vol. 1, pp. 15–26, 2015. [Online]. Available: https://doi.org/10.1016/j.csmssp.2015.05.001.

[45] P. A. Delgado-Arredondo, A. Garcia-Perez, D. Morinigo-Sotelo, *et al.*, "Comparative study of time-frequency decomposition techniques for fault detection in induction motors using vibration analysis during startup transient," *Shock and Vibration*, vol. 2015, 2015. [Online]. Available: https://doi.org/10.1155/2015/708034.

[46] N. E. Huang, Z. Shen, S. R. Long, *et al.*, "The empirical mode decomposition and the hilbert spectrum for nonlinear and non-stationary time series analysis," in *The Royal Society A - Mathematical, Physical and Engineering Sciences*, The Royal Society, vol. 454, The Royal Society, 1998, pp. 903–995.

[47] Z. Wu and N. E. Huang, "Ensemble empirical mode decomposition - a noise assisted data analysis method," *Advances in Adaptive Data Analysis*, vol. 1, no. 1, pp. 1–41, 2009. [Online]. Available: https://doi.org/10.1142/S1793536909000047.

[48] P. G. Kulkarni and A. D. Sahasrabudhe, "Investigations on mother wavelet selection for health assessment of lathe bearings," *The International Journal of Advanced Manufacturing Technology*, vol. 90, 9 - 12 2017. [Online]. Available: https://doi.org/10.1007/s00170-016-9664-3.

[49] R. Yan, "Wavelet selection criteria for non-stationary vibration analysis in bearing health diagnosis," University of Massachusetts, 2007.